Available online at www.sciencedirect.com
SCIENCE DIRECT®
Journal of Organometallic Chemistry 667 (2003) 66–72
Journal of Organometallic Chemistry
www.elsevier.com/locate/jorganchem

Modelling S_N2 nucleophilic substitution at silicon by structural correlation with X-ray crystallography and NMR spectroscopy

Alan R. Bassindale [a,*], David J. Parker [a], Peter G. Taylor [a,*], Norbert Auner [b], Bernhard Herrschaft [b]

[a] Department of Chemistry, Open University, Walton Hall, Milton Keynes MK7 6AA, UK
[b] Institut für Anorganische Chemie, Johann Wolfgang Goethe Universität, Marie Curie Strasse 11, D-60439 Frankfurt am Main, Germany

Received 9 September 2002; received in revised form 7 November 2002; accepted 7 November 2002

Abstract

The X-ray crystal structures of four 1-(halodimethylsilylmethyl)-2-quinolinones have been measured and used to model the reaction profile for nucleophilic substitution at silicon. Similar structural correlations have been performed in solution, the percentage Si–O bond formation being obtained from the ^{13}C chemical shifts of the quinolinone carbons and the extent of pentacoordination from the ^{29}Si chemical shift of the silicon. Excellent agreement is obtained between the two methods confirming the validity of the NMR technique for structural correlation in solution.

Keywords: Silicon; Pentacoordinate; NMR; X-ray study; Nucleophilic substitution; Structural correlation

1. Introduction

Crystal structure correlations, first used by Dunitz and Bürgi, have been used to map the trajectory of a variety of nucleophilic substitutions [1]. The crystal structures of a range of structurally similar compounds are sequenced on the basis of key crystal data (usually inter-atom distances) so that a gradual deformation is observed. Each structure represents a frozen snapshot of the substitution at a particular point on the modelled reaction profile. Application of this methodology to nucleophilic substitution at silicon shows that formation of the nucleophile–silicon bond is accompanied by lengthening of the silicon-leaving group bond via a trigonal-bipyramidal structure with the non-participating groups equatorial [2–5]. For example, Baukov [3] and Pestunovich [4] separately examined the crystal structures of a range of related *N*-(amidomethyl)-halosilanes (**1**) (Scheme 1). They found that the Si–O and Si–X bond lengths were related via a hyperbolic function, which was accompanied by a regular change of the position of the silicon atom relative to the plane of the three equatorial carbon atoms.

We sought to develop a method that would enable similar structure correlations to be obtained in the solution phase, using ^{13}C and ^{29}Si NMR spectroscopy as the monitoring tools [6,7]. The first systems studied were based on substituted 2-pyridone ligands (**2**). Variation of R and X led to a series of compounds with differing extents of O–Si bond formation and Si–X bond cleavage. The extent of bond formation could be measured from the change in ^{13}C chemical shift of the aromatic ring carbons, using model compounds to define the limiting cases of 0 and 100% Si–O bond formation. The degree of pentacoordination could be measured from the ^{29}Si chemical shift. A plot of the extent of pentacoordination versus the extent of Si–O bond formation maps the extent of nucleophilic substitution in solution. An increase in the extent of Si–O bond formation leads to an increase in pentacoordination until about 50% formation. After this the extent of pentacoordination decreases. Unfortunately, the pyridones employed could not be analysed by X-ray crystallography, so it was not possible to compare the structure in the solid and solution phase. The present paper

* Corresponding authors. Tel.: +44-1908-652-512; fax: +44-1908-858-327.
E-mail address: p.g.taylor@open.ac.uk (P.G. Taylor).

0022-328X/02/$ - see front matter
PII: S0022-328X(02)02130-7

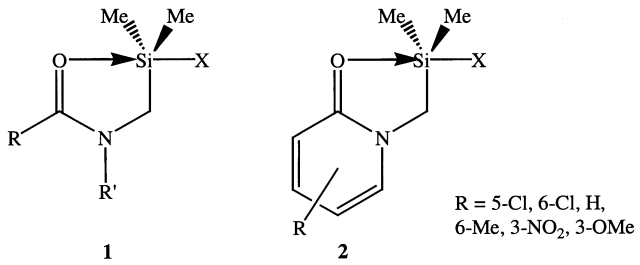

Scheme 1.

reports the preparation of a series of 2-quinolinone analogues **3a**–**3d** (Scheme 2), which can be analysed by both X-ray crystallography and solution NMR and thus provides a critical examination of this novel method of structure correlation.

2. Results and discussion

Treatment of 2-quinolinone with diethylaminetrimethylsilane gave the corresponding trimethylsilyl derivative. Reaction of this with chloro(chloromethyl)-dimethylsilane gave the chloro derivative **3b**, whereas treatment with (bromomethyl)(chloro)dimethylsilane gave the bromo derivative **3c**. The fluoro derivative, **3a**, was prepared by treating the chloro derivative, **3b**, with antimony trifluoride and the triflato derivative, **3d**, was prepared by treating **3b** with trimethylsilyl triflate. Fig. 1 shows the X-ray crystal structure of the fluoride **3a**, which is typical of the series **3a**–**3c**. The molecular structure of **3d** is shown in Fig. 2. Key data for the four compounds is presented in Table 1.

In the compounds **3a**–**3d** the two methyl substituents and the CH_2 group occupy the equatorial positions of a trigonal-bipyramid around the silicon. The apical positions are occupied by the 'incoming' oxygen atom of the quinolinone moiety and by the 'leaving' halide in **3a**–**3c** and the triflate group in **3d**. This behaviour, with the electronegative groups axial has been observed in many hypervalent silicon compounds [8–11]. The data in Table 1 show the ligand orientation to be rigid such that the whole arrangement can be described as two face sharing tetrahedra **T**o: C9–C10–C11–O and **T**x: C9–C10–C11–X (X = F^-, Cl^-, Br^-, $CF_3SO_3^-$).

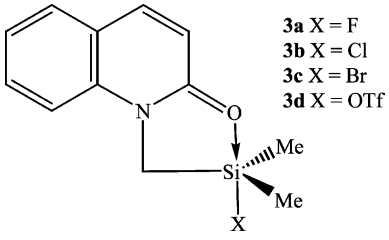

Scheme 2.

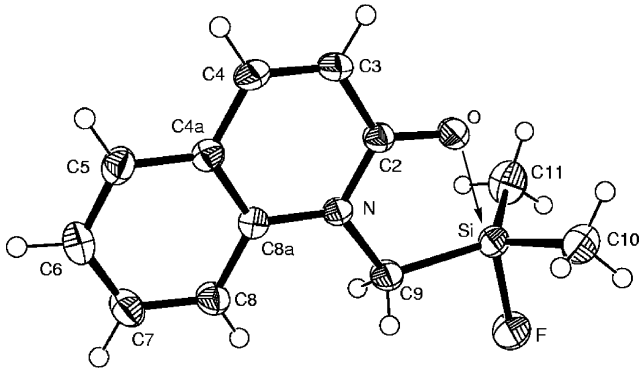

Fig. 1. ORTEP-representation of **3a**, envelopes are drawn at the 50% probability level. Selected bonding distances (Å) and bond angles (°) are given in Table 1.

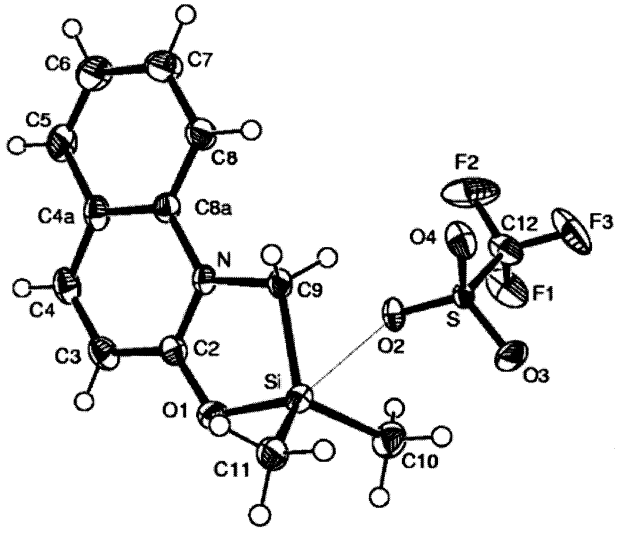

Fig. 2. ORTEP-representation of **3d**, envelopes are drawn at the 50% probability level. Selected bonding distances (Å) and bond angles (°) are given in Table 1. The solvent molecule of crystallisation has been omitted for clarity.

The carbon atoms C9, C10 and C11 lie at the corners of the common face of both tetrahedra and the structures **3a**–**3d** are snapshots of the migration of the silicon atom from the increasingly distorted tetrahedral hole of the **T**x tetrahedron through the basal plane C9–C10–C11 towards the centre of the nearly unchanged **T**o tetrahedron.

As expected, since fluoride is the poorest leaving group of the series, **3a** models the earliest point in the substitution process with the longest nucleophile–silicon distance. The Si–F bond is elongated slightly, being about 0.1 Å longer than a conventional Si–F bond. The silicon atom is situated 0.16(1) Å from the basal plane closer to the fluorine atom. Despite the weak oxygen interaction the geometry around the silicon is highly trigonal-bipyramidal as demonstrated by the sum of the equatorial bond angles being close to 360°. The O–Si–X

Table 1
Geometry of the silicon centres and key bond lengths (Å) and bond angles (°) of **3a**–**3d** in the crystal

	3a (X = F)	**3b** (X = Cl)	**3c** (X = Br)	**3d** (X = OTf)
SiC_3OX-polyhedron				
O···C9	2.57(4)	2.57(4)	2.57(3)	2.563(7)
O···C10	2.71(4)	2.72(4)	2.77(2)	2.87(5)
O···C11	2.72(8)	2.69(4)	2.72(2)	2.83(6)
C9···C10	3.26(3)	3.27(6)	3.23(3)	3.16(3)
C9···C11	3.25(6)	3.27(6)	3.27(3)	3.19(6)
C10···C11	3.19(6)	3.23(3)	3.183(1)	3.13(4)
C9···X	2.55(2)	2.93(2)	3.05(4)	2.79(5)
C10···X	2.66(4)	3.07(5)	3.23(3)	3.25(5)
C11···X	2.65(7)	3.08(3)	3.24(3)	3.08(4)
Δ [a]	0.163(1)	0.055(4)	−0.079(6)	−0.328(2)
Coordination at silicon				
Si–O	2.065(1)	1.939(4)	1.852(8)	1.745(3)
Si–X	1.675(1)	2.321(2)	2.648(3)	2.762(3)
ΣC–Si–C	357.7	359.8	359.4	350.9
O–Si–X	171.46(6)	171.2(2)	169.4(3)	160.4(3)
C2–O	1.271(2)	1.274(7)	1.29(1)	1.307(5)

[a] Δ, Perpendicular distance of the silicon centre from the least squares plane C9–C10–C11. A positive distance indicates a displacement towards the leaving group.

bond angle is less than the 180° expected for such nucleophilic substitution as a result of ring strain.

Chloride is a better leaving group than fluoride and thus in **3b** the oxygen is closer to the silicon by 0.12 Å. The Si–Cl bond is markedly stretched from its normal length by about 0.3 Å, the silicon atom has not left the **Tx** tetrahedron but has moved closer to the basal plane, now being just 0.055(4) Å from it. The sum of the equatorial bond angles shows that the silicon and the equatorial substituents are essentially planar.

The O–Si bond in **3c** is 0.11 Å shorter than in **3b**, leading to an Si–Br bond length which is 0.5 Å longer than a common Si–Br bond. The sum of the equatorial bond angles still shows a planar arrangement of equatorial substituents but the silicon atom has passed through the basal plane into the **T**o tetrahedron to a point 0.079(6) Å from it.

In **3d** (Fig. 2) the O–Si bond length is close to that of a standard Si–O bond, the silicon atom is near the centre of the **T**o tetrahedron 0.328(2) Å from the basal plane and the substitution is close to completion [3]. The nonbonding C–C distances in the basal plane remained nearly unchanged in **3a**–**3c** (mean: 3.238 Å), as did the nonbonding C–O distances (mean: 2.671 Å). The nonbonding C–C distances in **3d** are slightly contracted (mean: 3.160 Å) while the nonbonding C–O distances were widened (mean: 2.751 Å). The carbonyl bond distance C2–O, remains essentially constant within the series with a value between that expected for a single bond (1.36 Å) and a double bond (1.24 Å). Nevertheless, the small observed change is consistent with a reduction in bond order on Si–O bond formation. The interaction of the triflate group with the silicon is best described as electrostatic. The Si–O_{Tf} distance, 2.76 Å, represents only a weak coordination of the anion, leaving the silicon atom clearly four coordinate. Taking all next nearer, more electronegative neighbours (S, O, and F) into account within a radius of 4.6 Å, the coordination number rises to eleven. The crystal structure of **3d** appears as a rod like packing of chains of weakly C–H···F bridged, intramolecular donor stabilised $[R_3Si^+]/[OTf^-]$ cation–anion pairs.

Table 2 shows some of the equivalent data for the corresponding lactams **4a**–**4d** (Scheme 3) [3,5,12]. The similarity in geometric parameters suggests that the difference in nucleophilicity between the lactams and the quinolinones is small compared with the effect of changing the leaving group. Furthermore, the geometric constraints imposed by the ring systems must be similar in both cases.

The solution phase mapping procedure was carried out as described previously using compounds **5** and **6** (Scheme 4) as models for 0 and 100% Si–O bond formation, respectively, [7].

The percentage Si–O bond formation can be calculated by comparing the ^{13}C chemical shift of the aromatic ring carbons with those of the two limiting cases. All NMR data was obtained in $CDCl_3$ at 25 °C (0.1 mol l^{-1}) [13]. The data is averaged over all the ring carbons and is shown in Table 3 together with the percentage pentacoordination determined from the ^{29}Si chemical shift. As with the pyridine series, values of 28 and −40 ppm were used to anchor the chemical shift scale to a tetrahedral silicon with no Si–O interaction and a fully pentacoordinate silicon, respectively. *O*-Trimethylsilylated *N*-methylquinolin-2-one has a ^{29}Si chemical shift of 12.2 ppm and this was used to anchor the scale to a tetrahedral silicon with 100% Si–O bond formation. The data show that as the percentage O–Si bond formation increases to 50% so the percentage pentacoordination increases, after which the percentage pentacoordination decreases as observed with the pyridone complexes. The percentage Si–O bond formation for the 2-quinolinones is consistently higher than

Table 2
Key bond lengths (Å) and bond angles (°) of **4a**–**4d** in the crystal

	4a	**4b**	**4c**	**4d**
Si–O	2.31–2.46	1.95	1.80	1.75
Si–X	1.63–1.67	2.31	3.12	2.79
ΣC–Si–C	352.1–355.1	359.7	355.9	352.2
O–Si–X	171.3–174.0	171.2	162.6	165.0
C2–O	1.25	1.27	1.30	1.31
Δ [a]	0.23–0.30	0.06	−0.22	−0.31

[a] Δ, Perpendicular distance of the silicon centre from the least-squares plane C9–C10–C11. A positive distance indicates a displacement towards the leaving group.

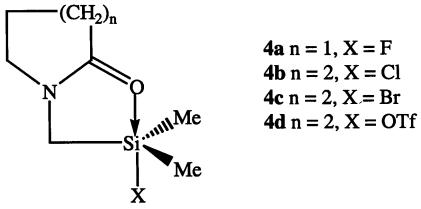

4a n = 1, X = F
4b n = 2, X = Cl
4c n = 2, X = Br
4d n = 2, X = OTf

Scheme 3.

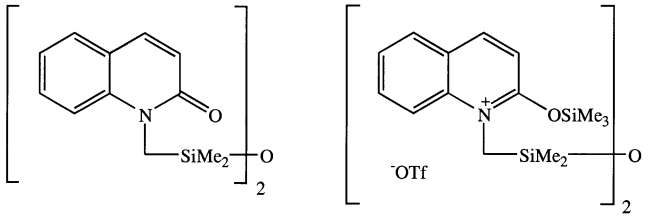

5 **6**

Scheme 4.

those of the corresponding unsubstituted 2-pyridones, as a result of further delocalisation of the positive charge on formation of the quinolinium species [8].

Fig. 3 shows a plot of the percentage Si–O bond formation as determined by NMR against the Si–O bond length as determined by X-ray crystallography. Considering the assumptions in the method and the differing bulk interactions within the solid and solution phase, there is an excellent correlation between the solution results and X-ray studies.

The percentage pentacoordination can be compared with the perpendicular distance of the silicon from the plane of the equatorial atoms, Δ. When the silicon is tetracoordinate, as in bromomethylchlorodimethylsilane [14] the displacement Δ, is 0.60 Å and when the silicon is perfectly pentacoordinate Δ should be zero. The displacement data mirrors the percentage of pentacoordination, the larger the Δ value, the smaller the percentage of pentacoordination. In fact, a plot of percentage of pentacoordination versus the magnitude of Δ is a reasonable straight line with a correlation coefficient of 0.96.

Any attempt to determine percentage of Si–O bond formation and pentacoordination from the X-ray crystal structure requires the use of model compounds to define 0 and 100%. Table 3 shows the percentage of pentacoordination obtained from Δ, using values of 0.60 Å for the displacement for 0% pentacoordination and zero for 100% coordination. Considering the assumptions, the agreement between the two methods is remarkable, with the difference being only 6–8%. The Si–O bond distance in methoxytrimethylsilane is 1.639 Å [15] and this value was used for 100% Si–O bond formation, however, the definition of 0% Si–O bond formation was not so straightforward. Whilst the crystal structure of **5** is not available, Ovchinnikov has measured the crystal structure of the phenoxy derivative, **7** (Scheme 5), which should have a similar structure [5]. Although the Si–O_{Ph} bond length, 1.711 Å, is close to the expected covalent bond length, the Si–$O_{carbonyl}$ distance is 2.367 Å demonstrating a small amount of coordination. As phenoxide is a poor leaving group, this coordination is likely to be due to the constraint of the silicon and $O_{carbonyl}$ groups being close together in different parts of the same molecule. As we should expect a similar residual coordination in **5**, thus, we chose to anchor one end of our scale using this value. The calculated percentage of Si–O bond formation based on the observed Si–O bond lengths are shown in Table 3. Again the correspondence is good, with the difference being again only 6–8%

In fact we would not expect the two methods to give identical values since there are likely to be specific interactions in the crystal which will not be present in solution. Similarly, the two sets of measurements were carried out at different temperatures, 100–200 K for the crystal structures and 298 K for the NMR method. The lower the temperature, the more coordinated the silicon [13], thus we would expect the percentage of Si–O bond formation for **3a** and **3b** to be greater from the X-ray measurements than from the NMR technique and to be smaller for **3c** and **3d**. A similar pattern should be observed for the percentage of pentacoordination. Whilst some of these trends are observed they are by no means perfect.

The solid state ^{29}Si-NMR spectrum of **3b** gave a single chemical shift of δ −39.6 which compared with the solution measurement (δ −38.4) shows that the geometry of the silicon in each state is very similar and that the crystal packing interactions are relatively small, at least in this molecule, compared with the influence of the coordinating groups. Further solid state NMR measure-

Table 3
Percentage Si–O bond formation and pentacoordination for **3a**–**3d**

	4	**3a**	**3b**	**3c**	**3d**	**5**
Percentage Si–O bond formation from NMR	0	35	63	78	93	100
Percentage pentacoordination from NMR	0	79	97	79	38	0
Percentage Si–O bond formation from X-ray	0	41	59	71	85	100
Percentage pentacoordination from X-ray	0	73	91	87	45	0

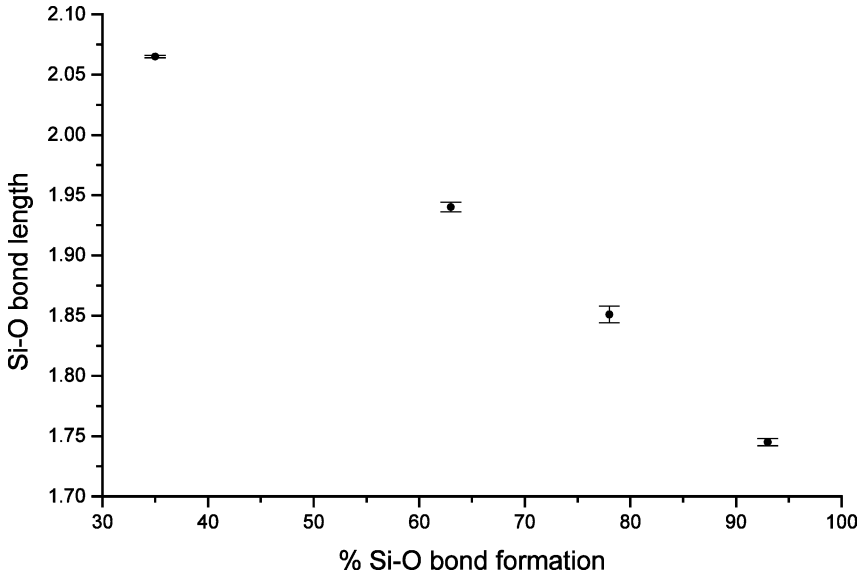

Fig. 3. A plot of percentage of Si–O bond formation as determined by NMR in the solution phase against the Si–O bond length determined in the crystal.

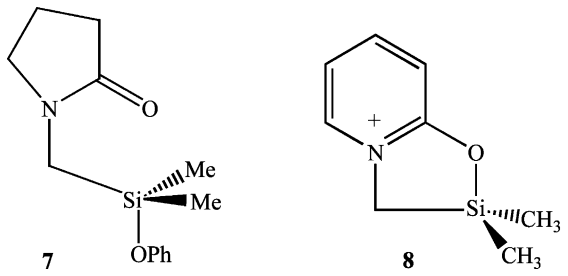

Scheme 5.

ments were limited by the moisture sensitivity issues of these compounds.

Another reason why the data may differ is because the model, **6**, used for 0% pentacoordination and 100% Si–O bond formation is inadequate because of the absence of ring strain. *Ab initio* Hartree–Fock calculations at the 6-31G** level suggest a Me_3Si–O bond length in **6** of 1.654 and a Δ value of 0.582 Å close to the values chosen to anchor the scale. However, the Si–O bond distance in **8** was calculated to be 1.728 Å with a Δ value of 0.431 Å. If such values were used to anchor the scale, the percentage of Si–O bond formation calculated from X-ray data would be larger; closer to those calculated using the NMR technique. Similarly, the values for the percentage of pentacoordination would also be closer.

3. Conclusion

The close correlation between the structural information obtained in solution and the solid state confirms that variation of the leaving group leads to a series of discrete pentacoordinate compounds whose structures can be probed in the solution phase using NMR spectroscopy. An alternative explanation of the solution behaviour is that, rather than a series of discrete compounds, the reaction mixture contains only fully tetracoordinate or pentavalent species in equilibrium, as shown in Scheme 6. As the substituent and leaving group changes so the equilibrium position first moves from favouring **9** to favouring **10** and then **11**. Such a series of equilibria would have to be rapid on the NMR timescale in order to give single sets of resonances in the NMR spectra of each nucleus. Since X-ray crystallography demonstrates that a continuum of structures occurs in the solid state and the data correlate well with structural data obtained in solution it is probable that a similar continuum of structures is possible in the solution phase and that any equilibria provide a minor contribution to the values of percentage Si–O bond formation and pentacoordination.

4. Experimental

4.1. General comments

The synthesis and characterising data for compounds **3a**–**3d**, **5** and **6** has already been reported [16], so discussion in this section shall be limited to the X-ray studies.

4.2. X-ray crystallographic studies of *3a*, *3b*, *3c*, and *3d*

All compounds were measured on a one circle diffractometer equipped with an imaging plate system as detector (IPDS 2.75) [17]. Graphite monochromated

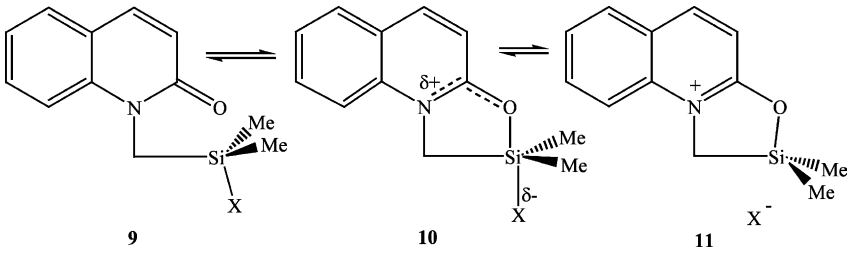

Scheme 6.

Table 4
Crystal data, data collection and refinement parameters for compounds **3a**–**3d**

	3a	**3b**	**3c**	**3d**
Formula	$C_{12}H_{14}FNOSi$	$C_{12}H_{14}ClNOSi$	$C_{12}H_{14}BrNOSi$	$C_{13}H_{14}F_3NO_4SSi\cdot\sim[0.5C_6H_6]$
Molecular weight	235.3	251.8	296.2	$365.4+\sim[0.5\times78.1]$
Colour	Colourless	Colourless	Colourless	Colourless
Morphology	Prism	Needle	Prism	Needle
Crystal size (mm)	$0.27\times0.27\times0.58$	$0.15\times0.15\times0.96$	$0.46\times0.46\times0.96$	$0.11\times0.11\times0.77$
Crystal system	Triclinic	Triclinic	Monoclinic	Triclinic
Space group	*P* (2)	*P* (2)	$P2_1/c$ (14)	*P* (2)
Unit cell dimensions				
a (Å)	7.091(1)	6.932(1)	10.005(2)	8.527(2)
b (Å)	8.750(2)	8.981(2)	7.213(1)	11.056(2)
c (Å)	9.872(2)	10.621(2)	17.692(4)	11.466(2)
α (°)	101.29(3)	100.47(3)	90	68.96(3)
β (°)	92.06(3)	91.04(3)	103.14(3)	75.41(3)
γ (°)	103.64(3)	111.06(3)	90	77.02(3)
V (Å^3)	581.6(2)	604.3(2)	1243.3(4)	965.5(4)
Z	2	2	4	1
D_{calc} (g cm^3)	1.344	1.384	1.583	1.330
F (000)	248	264	600	399
Temperature (K)	200	100	100	123
Reflections collected	2617	3040	2171	7931
Independent reflections	2617	3040	2171	3168
R_{int}	0.000	0.000	0.000	0.062
θ Range (°)	1.9–28.1	2.8–26.1	2.8–25.0	2.3–25.0
h Range	−9, 9	−8, 8	−11, 11	−10, 10
k Range	−11, 11	−11, 10	0, 8	−13, 13
l Range	0, 13	0, 13	0, 20	−13, 13
Observed data [$I>0.0\sigma(I)$]	1987	1878	1924	2660
R [$I>2\theta(I)$]	0.0408	0.1002	0.0855	0.0767
R_w [$I>2\theta(I)$]	0.1079	0.3275	0.02699	0.2314
S (goodness-of-fit on F^2)	1.02	1.15	1.13	1.08
N_{ref}	2617	2168	2171	3168
N_{par}	201	154	155	221

Mo–Kα radiation ($\chi=0.71073$ Å) was used. The data collection was performed in a ψ-rotation mode. A list of crystal data, data collection, structure solution and refinement parameters is provided in Table 4.

The raw intensity data was corrected for Lorentz and polarization effects with no attempts made to correct for absorption. Structure solutions were searched and refined by direct methods [18] (SHELXS 97_2) and difference Fourier analyses (SHELXL 97_2) [19], respectively, based on F^2. Atom form factors for neutral atoms were taken from the literature [20]. Second and third row elements were allowed to refine anisotropically, hydrogen atoms were assumed in idealised positions riding on their pivot atoms. The extent of solvent molecule occupancy in the crystal structure of **3d** has been calculated as around 50% from electron density measurements.

5. Supplementary material

Crystallographic data for the structures reported in this paper has been deposited with the Cambridge Crystallographic Data Centre as supplementary pub-

lication no. CCDC 132198-CCDC 132201. Copies of the data can be obtained free of charge on application to The Director, CCDC, 12 Union Road, Cambridge, CB2 1EZ, UK (Fax: +44-1223-336033; e-mail: data_request@ccdc.cam.ac.uk or www: http://www.ccdc.cam.ac.uk).

Acknowledgements

The support of the EPSRC for D.J.P. is gratefully acknowledged.

References

[1] (a) D. Britton, J.D. Dunitz, J. Am. Chem. Soc. 103 (1981) 2971; (b) H.B. Bürgi, J.D. Dunitz, Acc. Chem. Res. 16 (1983) 153.
[2] M.J. Barrow, E.A.V. Ebsworth, M.M. Harding, J. Chem. Soc. Dalton Trans., (1980) 1838.
[3] A.A. Macharashvili, V.E. Shklover, Y.T. Struchkov, G.I. Oleneva, E.P. Kramarova, A.G. Shipov, Y.I. Baukov, J. Chem. Soc. Chem. Commun. (1988) 683.
[4] V.F. Sidorkin, V.V. Vladimirov, M.G. Voronkov, V.A. Pestunovich, J. Mol. Struct. (Theochem.) 228 (1991) 1.
[5] Y.E. Ovchinnikov, A.A. Macharashvili, Y.T. Struchkov, A.G. Shipov, Y.I. Baukov, J. Struct. Chem. 33 (1994) 91.
[6] A.R. Bassindale, M. Borbaruah, J. Chem. Soc. Chem. Commun., (1991) 1499.
[7] A.R. Bassindale, M. Borbaruah, J. Chem. Soc. Chem. Commun., (1991) 1501.
[8] C.Y. Wong, J.D. Woollins, Coord. Chem. Rev. 130 (1994) 175.
[9] D. Kost, I. Kalikhman, in: Z. Rappoport, Y. Apeloig (Eds.), The Chemistry of Organic Silicon Compounds, vol. 2 (Chapter 23), Wiley, New York, 1998, p. 1339.
[10] R.R. Holmes, Chem. Rev. 96 (1996) 927.
[11] C. Chuit, R.J.P. Corriu, C. Reye, J.C. Young, Chem. Rev. 93 (1993) 1371.
[12] A.A. Macharashvili, V.E. Shklover, N.Y. Chernikova, M.Y. Antipin, Y.T. Struchkov, Y.I. Baukov, G.I. Oleneva, E.P. Kramarova, A.G. Shipov, J. Organomet. Chem. 359 (1989) 13.
[13] D. Kummer, S.H.Z. Abdel Halim, Anorg. Allg. Chem. 622 (1996) 57.
[14] Q. Shen, J. Mol. Struct. 112 (1984) 169.
[15] B. Csakvaki, Z. Wagner, P. Gomory, I. Hargitta, B. Rozsouda, F.C. Mulhoff, Acta. Chim. Acad. Sci. Hung. 90 (1976) 149.
[16] A.R. Bassindale, M. Borbaruah, S.J. Glynn, D.J. Parker, P.G. Taylor, J. Chem. Soc. Perkin Trans. 2 (1999) 2099.
[17] Stoe and Cie GmbH (1996), Imaging Plate Diffraction System Ver. 2.75, Darmstadt, Germany.
[18] G.M. Sheldrick, SHELXS 97_2. A Program for Crystal Structure Solution, University of Göttingen, Germany, 1998.
[19] G.M. Sheldrick, SHELXL 97_2. A Program for Crystal Structure Refinement, University of Göttingen, Germany, 1998.
[20] International Tables for Crystallography, Vol. C, Tables 4.2.6.8 and 6.1.1.4, Kluwer Academic Publishers, Dordrecht, The Netherland 1995.